Iraqi Journal of Physics, 2022 *Vol.20, No.2 , PP.38-52*
DOI: 10.30723/ijp.v20i2.991 *P-ISSN: 2070-4003*
E-ISSN: 2664-5548

Theoretical Investigations of Electronic and Optical Properties of Vanadium Doped Wurtzite Zinc Oxide from First Principle Calculation Method

Rezhaw A. Qadr[a 1,2], Dlear R. Saber [b1*], and Shujahadeen B. Aziz[c1]
[1]Department of Physics, College of Science, University of Sulaimani, Sulaymaniyah, Iraq
[2] Department of Physics, College of Education, University of Sulaimani, Sulaymaniyah, Iraq
[a]E-mail: rezhaw.qadr@univsul.edu.iq, [c]E-mail: shujahadeen.aziz@univsul.edu.iq
[b*]Corresponding author: dlear.saber@.univsul.edu.iq

Abstract

In this study lattice parameters, band structure, and optical characteristics of pure and V-doped ZnO are examined by employing (USP) and (GGA) with the assistance of First-principles calculation (FPC) derived from (DFT). The measurements are performed in the supercell geometry that were optimized. GGA+U, the geometrical structures of all models, are utilized to compute the amount of energy after optimizing all parameters in the models. The volume of the doped system grows as the content of the dopant V is increased. Pure and V-doped ZnO are investigated for band structure and energy bandgaps using the Monkhorst–Pack scheme's k-point sampling techniques in the Brillouin zone (G-A-H-K-G-M-L-H). In the presence of high V content, the bandgap energy decreases from 3.331 to 2.043 eV as seen by the band diagram. PDOS diagram was utilized to get the insight of the electronic structure of the atoms and the amount to which all energy bands contribute to a particular orbit of the atoms. As the V content grew, so did the PDOS for all of the states. The manipulation of bandgaps was carried out in a way that narrowing the bandgaps occurs, resulting in a redshift of the absorption spectrum in the IR region. At lower photon energies, the imaginary and real parts dielectric functions have increased. The effectiveness of V atoms on transmissivity especially in the low energy region of the V-doped ZnO perovskite has been verified compared to the other theoretical results.

Article Info.

Keywords:
ZnO, CASTEP, First principle calculation, Band structure, Optical properties.

Article history:
Received: Mar. 31, 2022
Accepted: Apr. 30, 2022
Published: Jun. 01,2022

1. Introduction

There are many uses of Zinc oxide (ZnO) semiconductors in a number of fields, including gas sensors, acoustic waves devices, transparent contacts, and medical biomaterials. An outstanding characteristic of ZnO-based semiconductors is its bandgap of 3.370 eV [1]. These materials are suitable photon materials known in ultraviolet and visible regions. The rationalization of designing modern optoelectronic devices relies on direct bandgap (DBG) manipulation in an attempt to produce barrier layers and quantum wells in heterostructures devices [1]. Tremendous studies on examining the optical and structural properties of various metals have been documented recently. Zinc oxide attracted attention due to the appropriate DBG of

3.37 eV which can be compared to the semiconductor material of gallium nitride (GaN). It has been reported that the binding energy of ZnO (60meV) is much higher than that of GaN semiconductor (24 meV) [2, 3]. The ZnO semiconductor is a well-known material characterized by non-toxicity, low cost, and abundant in resources. ZnO crystals appears in three forms: wurtzite, zinc blende, and rock salt ,as shown in Fig.1 [4].

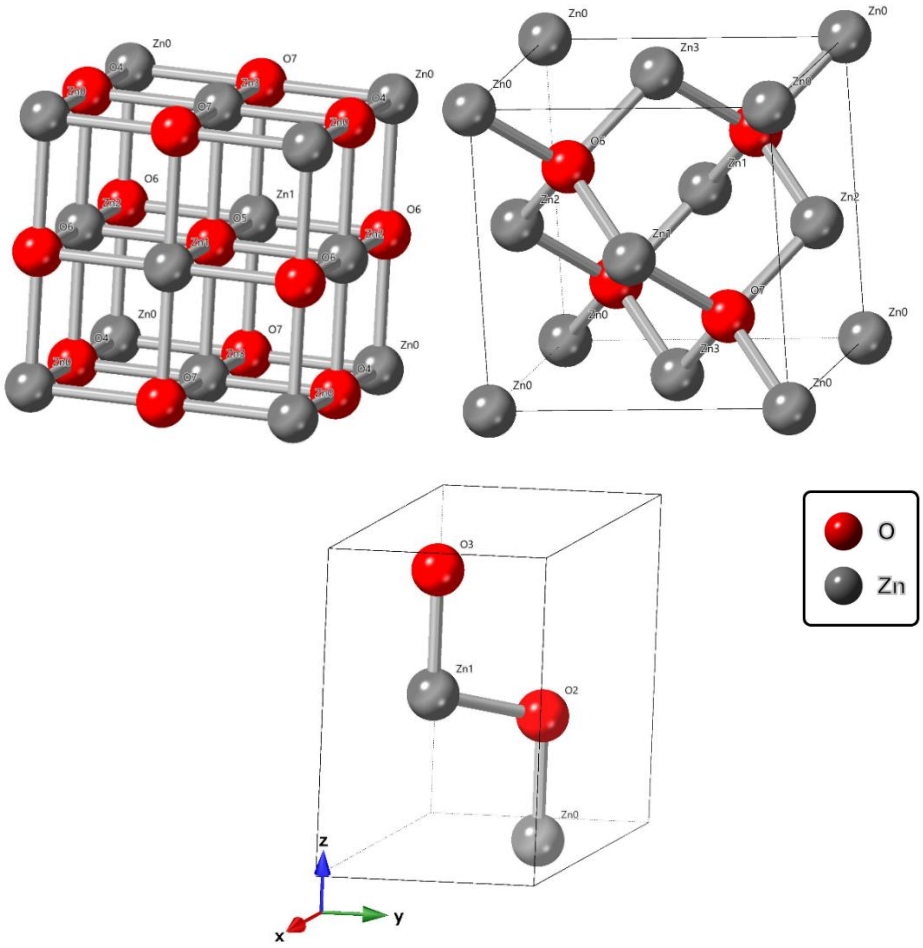

Figure 1: Schematic illustration of (a) rocksalt, (b) zinc-blend and (c) hexagonal wurtzite of ZnO structures.

Naturally occurring crystal structure of ZnO is the hexagonal wurtzite. Each Zn ion is surrounded by a tetrahedral tetrahedron of O ions in a hexagonal crystal structure with interpenetrating lattices [5]. The lattice parameters of hexagonal unit cell measured using X-ray diffraction under ambient circumstances are c = 5.2069 A^0, a= 3.2495A^0, and the axial ratio (c/a) is equal to 1.603; its density is equal to 5.605 g/cm^3[6]. The tetrahedral interaction between O^{-2} and Zn^{+2} ions causes polar symmetry along the hexagonal axis. Currently, in optical and mechanical manufacturing of devices, ZnO has widely been utilized in many fields [7] including light emitting and laser diodes [8-10], optoelectronic devices [11], photocatalysis [12], solar cells [13, 14], optoelectronic devices [15], and gas sensors [16]. This is owing to its wide bandgap which makes it weakly susceptible to visible light; thereby, only ultraviolet light is absorbed. Additionally, its conductivity and the number of carriers are both modest [17].

The doping of a transition metal into ZnO enables it to be applicable in optical and mechanical applications. Various experimental investigations of the optical and structural characteristics of transition metals and vanadium (V) V-doped ZnO have been documented. Maensiri et al. studied the optical properties of the V-doped ZnO prepared by sol-gel method [18]. The study verified that the bandgap (BG) of the V-doped ZnO samples was reduced upon the addition of V. Wang et al. [19] used both X-ray photoelectron and energy dispersive spectroscopy in the examination of the structural and optical properties of V-doped ZnO. It was clarified that V-doping makes all of the films possess a wurtzite structure and growth was predominately along the c-axis. Transmittance of the films was measured for the determination of the optical characteristics. Gherouel et al. [20] examined the optical and structural characteristics of V-doped ZnO prepared using spray pyrolysis technique. For varying controlled concentrations (1–5%) of vanadium, the BG energy varied between 3.17 and 3.25 eV. Within 300–1800 nm range the optical transmission and reflectance spectrum for each V-doped ZnO samples was recorded, with maximum transparency (80–90%) recorded in the visible range. Abaira et al. [21] performed optical and structural characteristics of V-loaded ZnO prepared by the sol-gel method. It was concluded that the loading of V from (2%-10%), widened the BG. The structural and optical properties of the widely loaded activated ZnO samples were identified from a theoretical point of view. Tan et al. [14]carried out optical and structural characteristics of Cadmium-doped ZnO. The prediction of the BG of a Cd-doped ZnO monolayer was documented using first-principle DFT in terms of the Hubbard U + local density approximation method. The negative sign of the formation energy of the doped sample emphasized that the is chemically stable.

Dai et al. [22] reported the Cu/Al-doped ZnO systems with optical characterization using the FPC generalized gradient approximation plane-wave pseudopotential approach in conjunction with the Hubbard U correction on the basis of DFT. To reduce the BG of ZnO, co-doping is the method of choice; consequently, causing the absorption edge of the systems to undergo red-shifting, and possessing the greatest absorption in the visible light. To explore electronic band structure, and optical characteristics of V-deped ZnO, the FPC based on DFT has been implemented in CASTEP [23]. Based on this approach, insight into optical properties of V-doping in ZnO at the scale of microscopic can be achieved.

In this research, hexagonal system of wurtzite ZnO was used since the wurtzite structure is most stable at ambient conditions and thus most common. There are three main targets in our research; (i) investigating the structural, and optical properties of pure, 4.16%, 6.25%, and 12.5% V-doped ZnO, (ii) studying theoretically, by the GGA+U approach, the properties of pure and V-doped ZnO structure, and (iii) comparing the findings with the other theoretical results of pure and V-doped ZnO materials.

2. Theoretical models and calculation methods

2.1 Speculative models:

The hexagonal system is the crystal structure of wurtzite ZnO, with the space group of P63mc. In ZnO structure, each Zn ion is surrounded by four O ions with three parameters of the unit cell which are: a = b = 3.249A^o, c = 5.205A^o [4]. To make the experimental results consistent, the supercells $Zn_{1-x}V_xO$ (2×2×1), (2×2×2), and (3×2×2), Fig. 2, were established to correspond to 4.1 %, 6.2 %, and 12.5 % of V doping, where V atoms can replace Zn atoms.

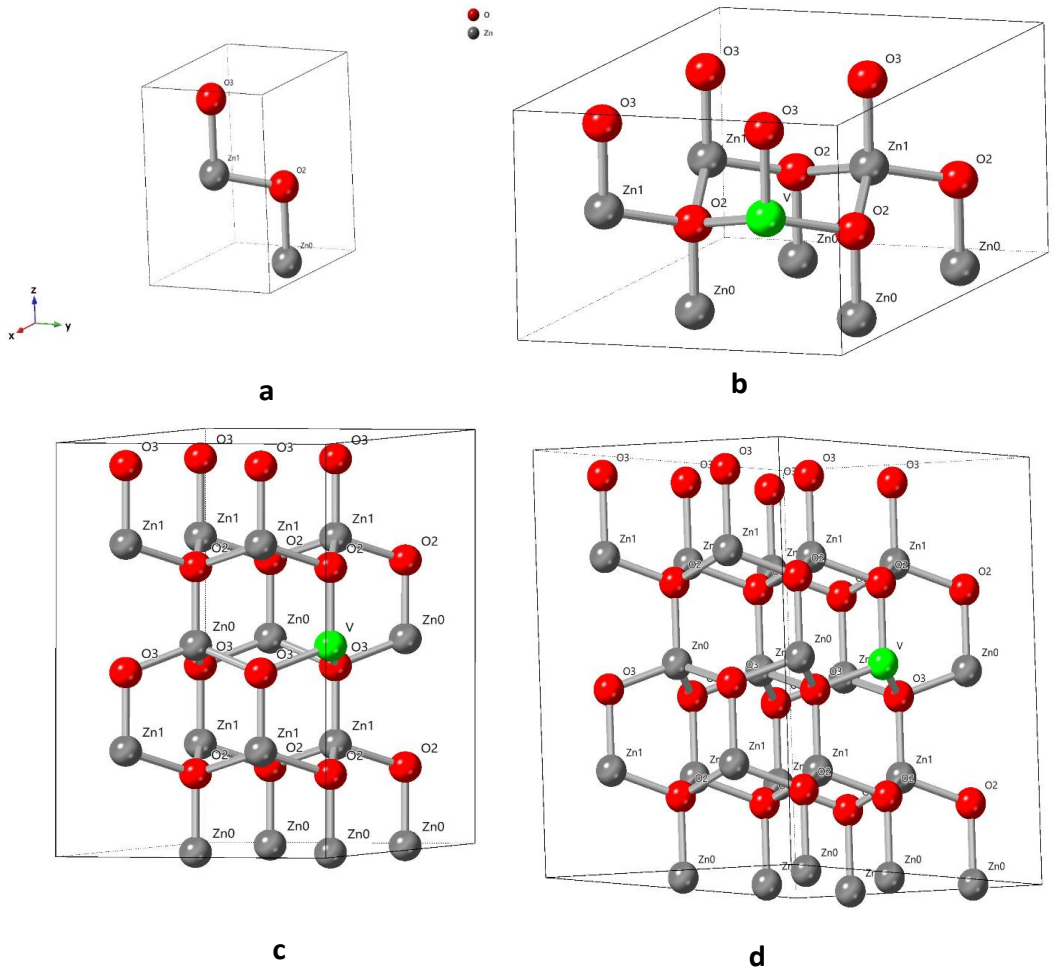

Figure 2: Designed Models for (a) ZnO, (b) $Zn_{0.958}V_{0.0417}O$, (c) $Zn_{0.9375}V_{0.0625}O$, and (d) $Zn_{0.875}V_{0.125}O$.

2.2 Calculation method

Taking the DFT into consideration and aiming at the plane-wave-pseudopotential (PWP) approach, the first-principles calculations (FPC) were done using the CASTEP code. The computations were based on DFT, as applied in the Materials Studio package's CASTEP software [23]. Fast calculations are the major feature of the applied approach because of its relatively high efficiency in which advances approximations of the shape of the orbitals is absent. The assumption is that the core of the ions is both inner electrons and nuclei; on the other hand, the valence electrons will interact and thus assure fast convergence of ion-electron potential. For electron-ion interaction investigation, the ultrasoft pseudo-potential (USP) was applied in addition to (GGA) and the electron exchange interaction proposed by Perdew–Burke–Ernzerhof (GGA-PBE) [23, 24]. The PWP method relies strongly on the assumption that almost all the physical and chemical characteristics of solids and molecules are governed by the valence electrons. This attempt is to rationalize the real atoms in the form of pseudo atoms, wherein just the valence electrons are involved in the self-consistent calculation (i.e., neglecting the impact of core electrons in the calculation). Therefore, the cost of computational calculation is reduced considerably [25]. Both the exchange and correlation energy possess impact; herein, has been dealt with within the GGA [26]. The certain valence electronic configurations used in the

current calculation are Zn $3d^{10}4s^2$, V $3d^3 4s^2$, and O$2s^2 2p^4$for the materials in a reciprocal space form.

At the conclusion of the self-consistent processing, the structure's total energy converges, the force exerted on the atoms is smaller than 0.03 eV/nm, and the stress deviation is less than 0.05 GPa.

Just to take into consideration, the k-points of the Brillouin zone are 5 5 4 (1×1×1 unit cells); 3 3 3 (2×2×1, 2×2×2, and 3×2×2 supercells). Here, the first optimization was the crystal structure, followed by calculations of the electronic structure, partial densities of state. Afterward, the optical characteristics were specified using the outcomes obtained from the structural parameters. The accurate description of the electronic structure of zinc oxides doped with the transition metal V and localized oxygen components is quantitatively performed from the GGA + U [26, 27]. However, it is much less than the experimental value (3.37 eV), which is due to the limitation of DFT in GGA [1]. Furthermore, the energy calculating for the first Brillouin zonula, was required to fulfill the particular k-instant pattern techniques of the Monkhorst–Pack design [27, 28]. The total energy of different k-point grids was computed for all compounds to reach a satisfied mesh, in order to ensure the accuracy of the whole results. The energy of the O 2p level and the Zn 3d level took the values Ud, Zn=10 eV, Us, Zn=0 eV Up, Zn=0, Up, O=7 eV, [2] in all of the systems.

3. Results and discussion

3.1 Lattice parameters study

To obtain the lattice parameters of ZnO, the optimization of geometric parameters was performed. The results are presented in Table 1. In the theoretical calculations, only a single crystal structural data of the compound of interest was taken into account. For example, for the un-doped ZnO, the lattice parameters took the values: a = b = 3.2492Aº and c = 5.2054Aº, and c/a=1.602. It was found that these lattice parameters are in good agreement with the following experimental values: a=b=3.25 Aº, c=5.207 Aº, and c/a=1.602 with a variance of less than 2% [21]. Despite this, the predicted lattice parameters and unit cell volumes were different (within 2 percent) from the calculated experimental value [4]. On the other hand, satisfactory agreement with existing theoretical values [11, 13, 20-23] was attained. While, it contradicted the results of Payne et al. [24]. It is worth noting that the GGA approximation has a built-in tendency to overestimate lattice parameters. As long as the computations are as accurate as they need to be, these types of mistakes are acceptable. Another interesting feature of the data is the tiny amount of variance between the theoretical and experimental values. First-principles computations have been shown to be accurate as a consequence. The volume and lattice parameters of the ZnO system in the a and c axes were found to increase as the quantity of V^{5+} ions in doping was increased. The doped system lattice properties and volume were somewhat higher than those of the parent ZnO system. This is caused by the indigence to calculate the electronic structure properties in which the lattice parameters are impacted.

When calculating the band gap for most systems, the limitations involved in the GGA approximation, make bandgap calculations inaccurate. Another cause of the present results is the repulsive interactions of the extra electrons of the V^{5+} ion that exists effectively. As a result of both factors impact, the volume of the doped sample rises as the amount of V-doping increases. From Table 1, it is obvious that different doping elements presents various impacts on the changing rate of the lattice constants a and c, and the ratio between them.

Table 1: Lattice parameters of pure ZnO and doped ZnO for different elements after geometry optimization.

Structure	a=b /A°	c/A°	V/A° ^{3}	c/a	Ref.
ZnO	3.247	5.202			[20]
ZnO:V 2%	3.261	5.326			
ZnO:V 6%	3.235	5.283			
ZnO:V 10%	3.250	5.210			
ZnO	3.2492	5.2054	47.5948	1.602	Present paper
ZnO:V 4.16%	3.25655	5.2402	48.1270	1.609	
ZnO:V 6.25%	3.26164	5.2530	48.3915	1.610	
ZnO:V 12.5%	3.28078	5.2870	49.2810	1.611	

3.2 Band structure and density of state studies

The work conducted in this research specified the band structure along a high symmetry direction in the Brillouin zone (G-A-H-K-G-M-L-H) for pure and V-doped ZnO. When determining a material's characteristics, it is important to accurately determine both its density of states (DOS) and its BG structure. In addition, the likelihood of electrons occupying certain energy ranges may be calculated from the shape of the electronic band (that is energy bands). As a result, the bandgap refers to the energy ranges that are unusable. The electronic bandgap may be measured in insulators and semiconductors by comparing the maximum of the valence band (VB_{Max}) with the minimum of the conduction band (CB_{Mim}). The electronic band structure computations are useful in determining the probable transition of electrons from VBM to CBM. It is intuitive that the valence band lies below the Fermi state (E_f) at 0 eV, and the CB locates above the BG energy.

From Fig. 3, a direct G-G, transition BG energy of 3.331 eV for super-cells including, $Zn_{0.9583}V_{0.04166667}O$ and $Zn_{0.9375}V_{0.0625}O$ and the band structure calculated along the symmetry direction in the Brillion zone (G-A-H-K-G-M-L-H) were recorded. Located at the G point, the valence and conduction bands both have a straight G-G transition. This suggests the existence of p-type semiconductors of $Zn_{0.9583}V_{0.04166667}O$ and $Zn_{0.9375}V_{0.0625}O$. It is principally accepted that the direct nature of the bandgap contains a transition of an electron from the VB to the CB without phonons assistance which is mostly free of losing incident energy during transitions. The bottom 10 bands (occurring around -9 eV) are related to Zn 3d levels. The next 6 bands from -5 eV to 0 eV correspond to O 2p bonding states [29, 30]. The basis of DFT allows the designing of doped ZnO characterized by low bandgap materials accompanied by a direct bandgap. The BG energy was reduced from 2.321 to 2.279 eV upon doping ZnO with 4.16 and 6.25% V, respectively. Ultimately, the direction in the Brillouin zone (G-A-H-K-G-M-L-H) and the direct transition, G-to-G, of the supercell $Zn_{0.875}V_{0.125}O$, are evidence of the formation of p-type semiconductors.

This model tells that the bandgap can be reduced to the energy of 2.055eV. Fig.3(a) demonstrates that the value of the direct band in parent ZnO is lower than the experimental value (3.37 eV). In other words, the theoretical values of the BG energy are lower than the experimental values in all cases. This might be owing to the lack or at least poor description of strong Coulomb correlation and exchange interaction between electrons. Importantly, an obvious notice is that the calculated bandgap of the present and previous studies are in good agreement as presented in Table 2.

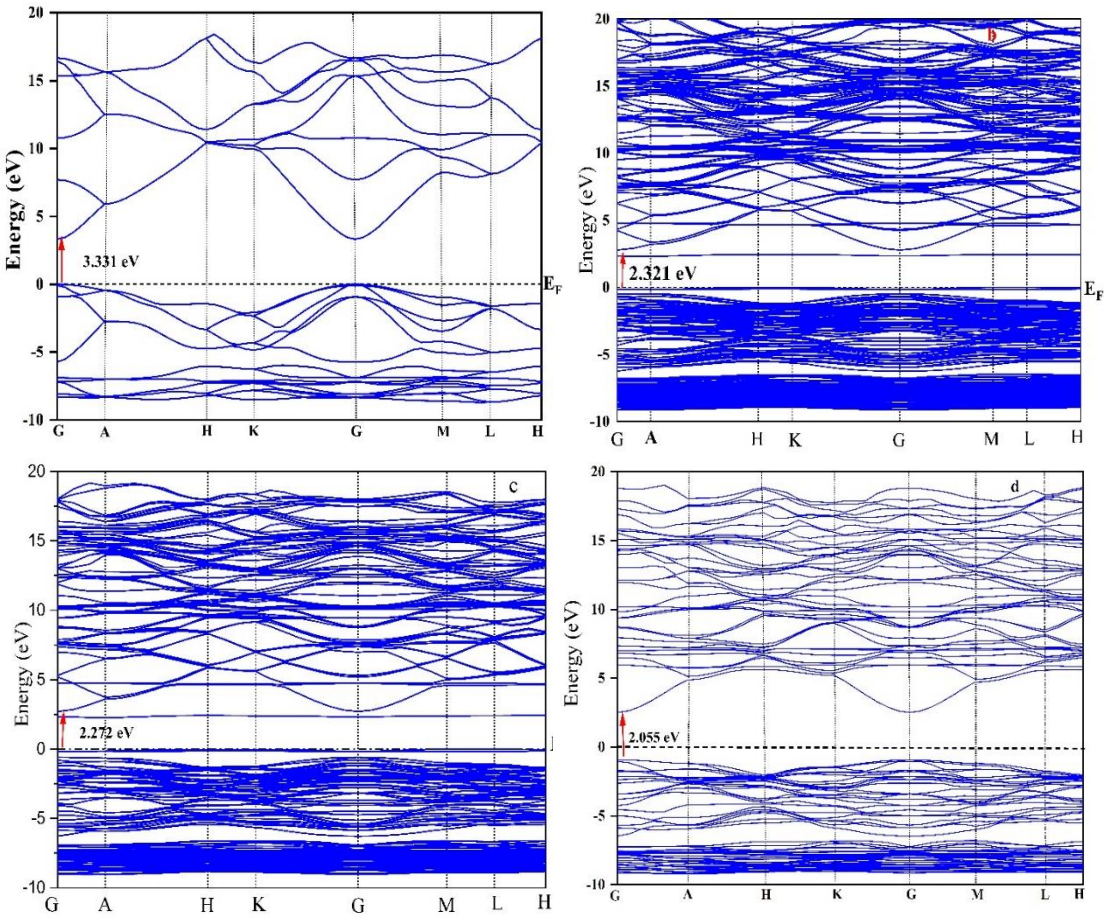

Figure 3: The E-K (Band Structure) diagram for (a) ZnO; (b)$Zn_{0.958}V_{0.0417}O$, (c) $Zn_{0.9375}V_{0.0625}O$, and $Zn_{0.875}V_{0.125}O$.

Table 2: The DBG energy of pure ZnO and doped ZnO for different elements after geometric parameters optimization.

Structure	E_g/eV	Functional	Computer code	Ref.
ZnO	3.40	GGA+U	CASTEP	[1]
ZnO:In 5.55%	2.91			
ZnO:V - 1%	3.17	Experimental		[8]
ZnO:V - 2%	3.23			
ZnO:V - 3%	3.25			
ZnO:V - 4%	3.20			
ZnO:V- 5%	3.22			
ZnO	4.00	LDA+U	CASTEP	[9]
ZnO	3.331	GGA+U	CASTEP	Present work
ZnO:V 4.16%	2.294			
ZnO:V 6.25%	2.272			
ZnO:V 12.5%	2.043			

The partial density of states (PDOS) of both parent ZnO, $Zn_{0.9583}V_{0.04166667}O$, $Zn_{0.9375}V_{0.0625}O$, and $Zn_{0.875}V_{0.125}O$ supercells are plotted against energy, as exhibited in Fig. 4. Introducing the V atoms into the ZnO lattice results in existing of primarily O $2s^2 2p^4$state, and V $3d^2$ in the top of valence, forming V-O bonds besides

Zn-O bands. In Fig. 4b, PDOS was applied to analyze the electronic structure deeply providing a contribution of the energy bands in a certain atomic orbital.

In parent ZnO, both Zn $3d^{10}4s^2$, and O$2s^2 2p^4$states contribute mostly to the valance bands between −5.5 and 0eV, and Zn $3d^{10}4s^2$, V $3d^3 4s^2$, and O$2s^2 2p^4$states are involved in the conduction bands ranging between 3.318 and 12.05 eV.

For super-cells, there are additional contributions of V $3d^3 4s^2$ states. The localized V $3d^2$ energy state substitutes dopant V ions for Zn which localizes within the Fermi level between -0.7 to 0.5 eV. The presence of V $3d^3 4s^2$ within the bandgap from 1.6 to 3eV leads to the reduction of the bandgap. The existence of these states between 4 to 8 eV is evidenced. Consequently, the PDOS of all these states increases with increasing the quantity of V in the doping process as shown in Fig.5 (a-c).

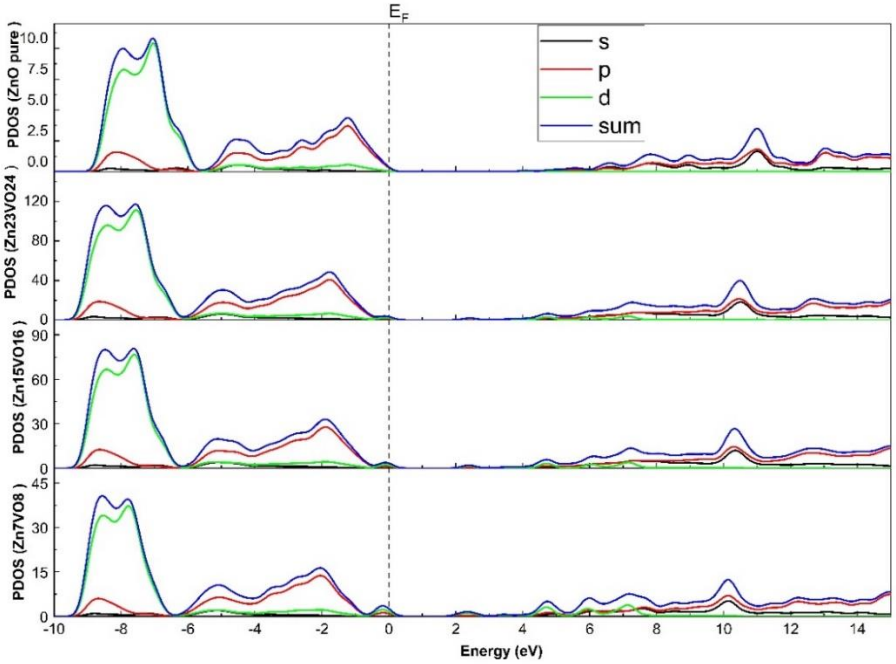

Figure 4: The total PDOS for (a) ZnO, (b)$Zn_{0.958}V_{0.0417}O$, (c) $Zn_{0.9375}V_{0.0625}O$, and $Zn_{0.875}V_{0.125}O$.

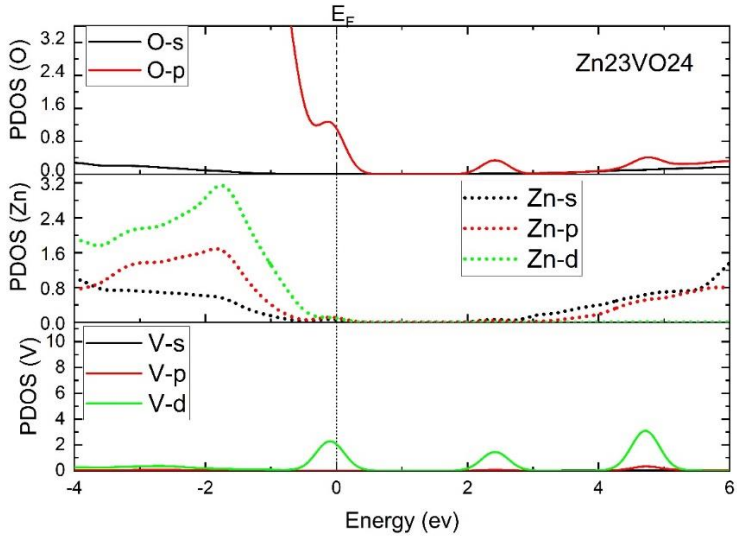

Figure 5(a): The PDOS of s, p, and d-state O, Zn, and V in $Zn_{0.958}V_{0.0417}O$ supercell.

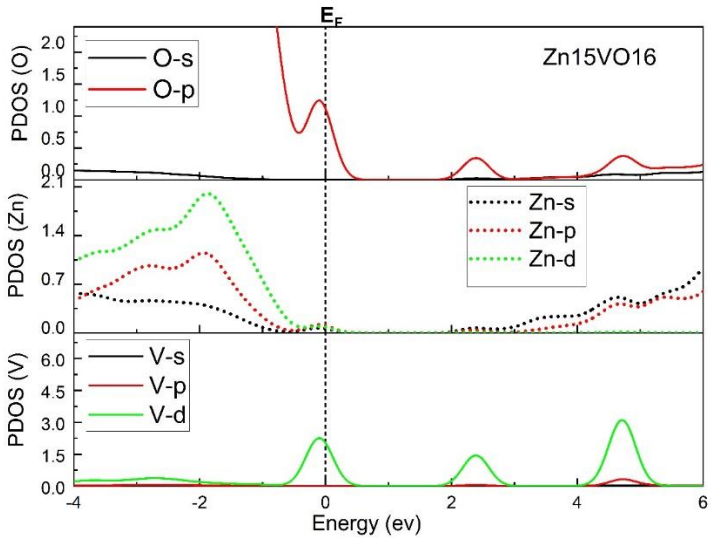

Figure 5(b): The PDOS of s, p, and d-state O, Zn, and V in $Zn_{0.9375}V_{0.0625}O$ supercell.

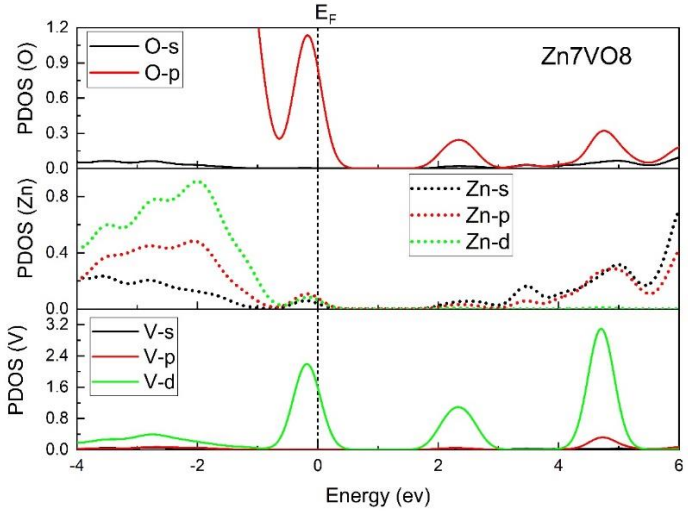

Figure 5(c): The PDOS of s, p, and d-state for O, Zn, and V in $Zn_{0.875}V_{0.125}O$ supercell.

3.3 Optical properties

Crystal band structure and optical qualities are reflected in the dielectric function, which may be thought of as the point at which electronic transition and electronic structure meet. The solid-state technique states that the complex dielectric function $\varepsilon(\omega) = \varepsilon_1(\omega) + i\varepsilon_2(\omega)$can express the optical properties of semiconductor materials [31]. On the other hand, the imaginary part results from the transition between the CB and the VB. Theoretically calculating momentum matrix components for filled and non-filled levels and Kramers-Kronig dispersion relations yields both the real $\varepsilon_1(\omega)$and imaginary $i\varepsilon_2(\omega)$ portions of dielectric functions, respectively [32, 33]. According to quantum mechanics, the system's photon-electrons interact through time-dependent disturbances in the system's ground electronic state. The absorption or emission of photons is what triggers transitions between occupied and unoccupied states in a quantum system. Furthermore, from $\varepsilon_1(\omega)$ and $i\varepsilon_2(\omega)$, extraction of other optical properties is obtainable. The optical properties from the density functional theory are achievable, for instance, the dielectric function, absorption coefficient, and refractive index [34] can be calculated from Eqs. (1,2,3,4,5) [12, 15, 34-37].

$$\varepsilon_1(\omega) = \frac{2}{\pi}\rho_0 \int_0^{\infty} \frac{\omega' \varepsilon_2(\omega)}{\omega'^2 - \omega^2} d\omega \qquad (\mathbf{1})$$

$$\varepsilon_2(\omega) = \frac{C}{\omega^2} \sum_{V,C} \int_{BZ} \frac{2}{(2\pi)^3} |M_{CV}(k)|^2 . \delta\left(E_C^k - E_V^k - \hbar\omega\right) d^3k \qquad (\mathbf{2})$$

$$\alpha(\omega) = \sqrt{2}\omega \left[\sqrt{\varepsilon_1^2(\omega) + \varepsilon_2^2(\omega)} - \varepsilon_1(\omega)\right]^{\frac{1}{2}} \qquad (\mathbf{3})$$

$$n(\omega) = \left[\sqrt{\varepsilon_1(\omega)^2 + \varepsilon_2(\omega)^2} + (\omega)\right]^{\frac{1}{2}} / \sqrt{2} \qquad (\mathbf{4})$$

$$k(\omega) = \left[\sqrt{\varepsilon_1(\omega)^2 + \varepsilon_2(\omega)^2} - (\omega)\right]^{\frac{1}{2}} / \sqrt{2} \qquad (\mathbf{5})$$

where $\hbar$ and K are Planck constant and the inverted lattice, respectively, and ω and ρ_0 are angular frequency and the density of the medium, respectively. The δ represent the displacement, $|M_{CV}(k)|^2$ refers to the momentum transition matrix elements, and E_V^k and E_C^k are the VBM and CBM energy, respectively.

Fig.6 (a) illustrates a sharp decrease of the real component $\varepsilon_1(\omega)$ in a relatively low energy region, reaching 1.98 eV where for V-doped systems ($Zn_{0.9583}V_{0.04166667}O$; $Zn_{0.9375}V_{0.0625}O$; $Zn_{0.875}V_{0.125}O$.) achieve negative values of $\varepsilon_1(\omega)$ i.e., − 5.07 at 0.997 eV, − 4.5 at 0.992 eV and – 1.85 at 1.04 eV, respectively. The increase of $\varepsilon_1(\omega)$ toward the positive region in the high range of energies is seen. The polarization and dispersion of electromagnetic radiations were negligible when the energy of the input photon reaches 20.7 eV, and the $\varepsilon_1(\omega)$ for the V-doped ZnO systems seem to be parallel to the energy axis. Fig. 6 (b) shows that parent ZnO possesses four peaks at 4.966 eV, 9.456 eV, 13.167 eV, and 15.327 eV matching the other theoretical results of (4.4, 8.9, 12.5, and 14.8 eVs)[16]. ZnO's DOS and energy band structure interpretation suggests that the 1st peak is mostly the optical response to the transition from O 2p state electron at the VB to Zn 4s level at the CB in ZnO. Two of the four peak occurrences in VB are caused by transitions between the Zn 3d state and the O 2s state due to Zn 3d and O 2p transitions. V 3d states and Zn 4s states in the conduction band are interband transitioned, resulting in a peak (0.21-0.25 eV) in the low region, where the change in position corresponds to the localized degree of impurity band. At the high energy range, the remaining three primary peaks remain in their original locations, indicating that there has been no transition. It is notable, however, that just the first primary peak has altered its location, indicating that ZnO's low-energy area has been effectively doped. However, even if the final peak is due to a mixed transition, it is seen that the loaded sample not only moved the absorption peaks to lower energies but also reduced the sharpness of their appearance. It is more effective at absorbing low-energy radiation because it has a smaller absorption edge than pure ZnO. Fig.4 indicates that the bandgap has narrowed dramatically, resulting in a reduced absorption edge. Doping ZnO with V, on the other hand, resulted in a decrease in energy bandgaps.

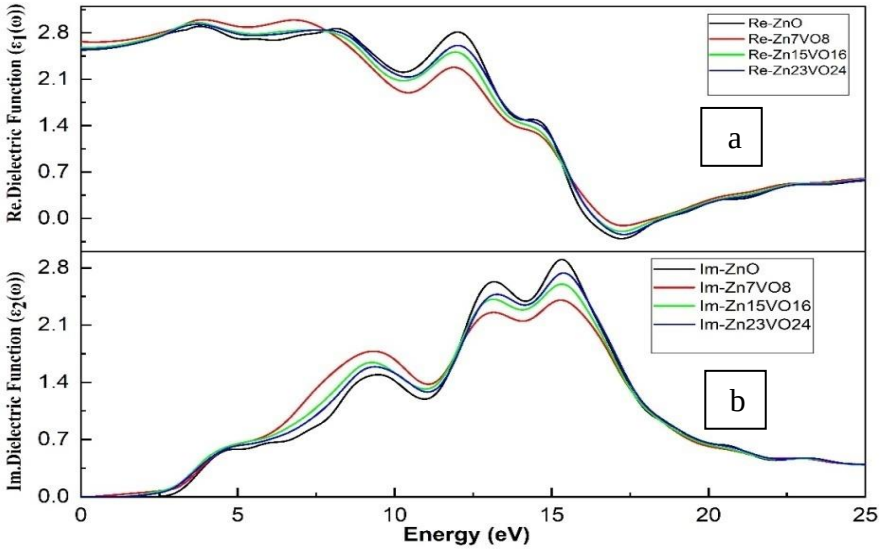

Figure 6: (a) Real part of dielectric function $\varepsilon_1(\omega)$, (b) Imaginary part of dielectric function.

The optical absorption spectrum is the vital tool that is mainly focused on. The absorption coefficients of ZnO corresponding to various quantities of V are presented in Fig.6. A redshift is seen in the absorption edge of V-doped ZnO compared to that of the parent ZnO. The absorption edge experiences shifting towards the lower energy as a red-shift, due to the reduction of the BG. The response of peaks belongs to the electron transitions between the Zn-3d and O-4s states. In fact, the parent ZnO is not a strong absorber in the IR region; however, it is a good absorber in the UV region. The process of V-doping enhances IR absorption significantly.

The energy of visible light is well assumed to be between 1.65 and 3.1 eV. In Fig. 7, it is noted that the V-doped ZnO has strong adsorption near UV regeneration. From the right side of Fig. 7, it is seen that the pure and V-doped ZnO also have poor absorption in the visible and infrared regions. The strong absorption in visible and near-ultraviolet regions is due to the electron inter-band transitions in vanadium 3d states [12]. The inter-band electronic transition of the states V-3d and Zn-4s in the conduction band can cause weak absorption in the infra-red regions. The system has a strong absorption at (15.9 eV-16.59 eV) for pure and V-doped ZnO.

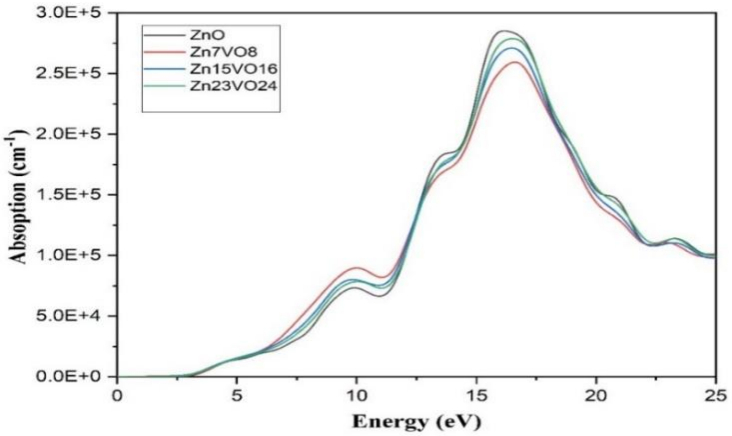

Figure 7: Absorption coefficient of pure and V-doped ZnO.

The extinction coefficient (k) and the complex refractive index (n), Fig.8, are dependent on energy (frequency). Both the n and the k must be calculated to establish how light interacts with atoms. The local polarizability and density of the materials considerably influence both attributes. Eqs. (4 and 5) may be used to get the n(ω) and the k(ω). A comparison of the characteristics of parent ZnO and V-doped ZnO is shown in Fig.8. The k and the n, both of which assess a material's transparency, are well-defined subsets of the complex refractive index (attenuation of electromagnetic waves inside the material is related to the imaginary part of the refractive index) When comparing the refractive indices of the parent and V-doped ZnO, the latter has lower refractive index. The dynamic refractive index n(ω) for the parent is low compared with the V-doped ZnO in the range of 0-2 eV, and beyond that, it increases slightly within the visible region. The n of the relatively high-energy region does not change (plateau). n changes from semiconducting to metallic ZnO following the introduction of V are confirmed by this shift in n.

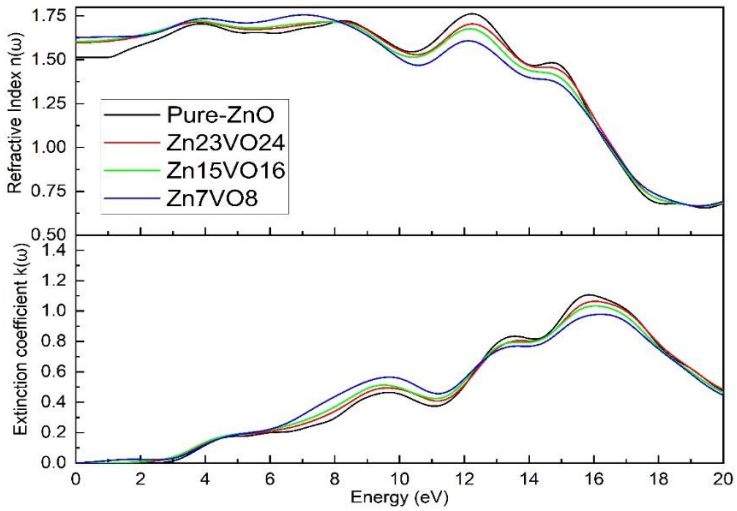

Figure 8: Refractive index n(ω) and extinction coefficient k(ω), for pure and V-doped ZnO with different contents.

4. Conclusions

In the conclusion, it seems that a first-principles implementation is necessary to assess the electrical, structural and optical feature of the parent and V-loaded ZnO systems. According to the findings of the calculations, the bandgap of the pure and V-doped systems has shrunk from 3.318 to 2.055 eV as a consequence of the increased V amount. Increase of the V amount has led to a change in the optical transition between the VBM and CBM. Doping with V caused refractive index, extension coefficient, and the real and imaginary part dielectric function of the ZnO to be relatively high in the low energy range. An increase of V doping encourages a volume increase of ZnO. The redshift of the absorption spectrum is enhanced in the IR region when the V content was increased as an impurity.

Acknowledgments

We would like to thank Dr Dominik Jochym from Scientific Computing Department Building R116 STFC R. A. Laboratory, Harwell Campus, Didcot Oxfordshire OX11 0QX, for supporting the CASTEP code.

Conflict of interest

The authors have no contention of interest to affirm.

References

1. Sharma D.K., Shukla S., Sharma K.K., and Kumar V., *A review on ZnO: Fundamental properties and applications.* Materials Today: Proceedings, 2022. **49**(8): pp. 1-8.
2. Hou Q., Xi D., Li W., Jia X., and Xu Z., *First-principles research on the optical and electrical properties and mechanisms of In-doped ZnO.* Physica B: Condensed Matter, 2018. **537**: pp. 258-266.
3. Song D.M., Wang T.H., and Li J.C., *First principles study of periodic size dependent band gap variation of Cu doped ZnO single-wall nanotube.* Journal of molecular modeling, 2012. **18**(12): pp. 5035-5040.
4. Wong C.P.P., Juan J.C., Lai C.W., Johan M.R., and Lee K.M., *Zinc Oxide Nanomaterials-Based Supercapacitors.* Encyclopedia of Energy Storage, 2020. **4**: pp. 374-381.
5. Janotti A. and Van de Walle C.G ,.*Fundamentals of zinc oxide as a semiconductor.* Reports on progress in physics, 2009. **72**(12): pp. 1-29.
6. Vyas S., *A short review on properties and applications of ZnO based thin film and devices.* Johnson Matthey Technology Review, 2020. **64**(2): pp. 202.218-
7. Sahal M., Hartiti B., Ridah A., Mollar M., and Mari B., *Structural, electrical and optical properties of ZnO thin films deposited by sol–gel method.* Microelectronics Journal, 2008. **39**(12): pp. 1425-1428.
8. Jangir L.K., Kumari Y., and Kumari P., *Zinc oxide-based light-emitting diodes and lasers*, in *Nanostructured Zinc Oxide*. 2021, Elsevier. p. 351-374.
9. Luan Z., Sun D., Tan C., Tian X., and Huang Y., *First-principles calculations of electronic structure and optical properties of Be-doped ZnO monolayer.* Integrated Ferroelectrics, 2017. **179**(1): pp. 84-94.
10. Rahman F., *Zinc oxide light-emitting diodes: a review.* Optical Engineering, 2019. **58**(1): pp. 1-20.
11. Chen H., Qu Y., Sun L., Peng J., and Ding J., *Band structures and optical properties of Ag and Al co-doped ZnO by experimental and theoretic calculation.* Physica E: Low-dimensional Systems Nanostructures, 2019. **114**: pp. 1-6.
12. Wang Q.-B., Zhou C., Wu J., and Lü T., *A GGA+ U study of the optical properties of vanadium doped ZnO with and without single intrinsic vacancy.* Optics Communications, 2013. **297**: pp. 79-84.
13. Vittal R. and Ho K.-C., *Zinc oxide based dye-sensitized solar cells: A review.* Renewable Sustainable energy reviews, 2017. **70**: pp. 920-935.
14. Tan C., Sun D., Xu D., Tian X ,.and Huang Y., *Tuning electronic structure and optical properties of ZnO monolayer by Cd doping.* Ceramics International, 2016. **42**(9): pp. 10997-11002.
15. Xia C., Wang F., and Hu C., *Theoretical and experimental studies on electronic structure and optical properties of Cu-doped ZnO.* Journal of alloys compounds, 2014. **589**: pp. 604-608.
16. Aroutiounian V., *Zinc Oxide Gas Sensors.* Journal of Contemporary Physics, 2020. **55**(4): pp. 323-333.
17. Xie A., Yang D., Li X., and Zeng H., *Lattice restraint induced ultra-large bandgap widening of ZnO nanoparticles.* Journal of Materials Chemistry C, 2019. **7**(29): pp. 8969-8974.

18. Maensiri S., Masingboon C., Promarak V., and Seraphin S., *Synthesis and optical properties of nanocrystalline V-doped ZnO powders.* Optical Materials, 2007. **29**(12): pp. 1700-1705.
19. Li-Wei W., Zheng X., Li-Jian M., Teixeira V., Shi-Geng S., and Xu-Rong X., *Influence of concentration of vanadium in zinc oxide on structural and optical properties with lower concentration.* Chinese Physics Letters, 2009. **26**(7): pp. 1-4.
20. Gherouel D., Dabbous S., Boubaker K., and Amlouk M., *Vanadium doping patterns in ZnO lattices in the lattice compatibility theory framework.* Materials science in semiconductor processing, 2013. **16**(6): pp. 1434-1438.
21. Abaira R., El Ghoul J., Fabbri F., Matoussi A., ElMir L., and Salviati G., *Synthesis and enhanced effect of vanadium on structural and optical properties of zinc oxide.* Optical Quantum Electronics, 2016. **48**(2): pp. 1-10.
22. Dai J., Suo Z., Li Z., and Gao S ,.*Effect of Cu/Al doping on electronic structure and optical properties of ZnO.* Results in Physics, 2019. **15**: pp. 1-7.
23. Clark S.J., Segall M.D., Pickard C.J., Hasnip P.J., Probert M.I., Refson K., and Payne M.C., *First principles methods using CASTEP.* Zeitschrift für kristallographie-crystalline materials, 2005. **220**(5-6): pp. 567-570.
24. Payne M.C., Teter M.P., Allan D.C., Arias T., and Joannopoulos a.J., *Iterative minimization techniques for ab initio total-energy calculations: molecular dynamics and conjugate gradients.* Reviews of modern physics, 1992. **64**(4): pp. 1045–1097.
25. Perdew J.P., Burke K., and Ernzerhof M., *Generalized gradient approximation made simple.* Physical review letters, 1996. **77**(18): pp. 3865-3868.
26. Song D. and Li J., *First principles study of band gap of Cu doped ZnO single-wall nanotube modulated by impurity concentration and concentration gradient.* Computational materials science, 2012. **65**: pp. 175-181.
27. Peng Y., Wei S., Xia C., and Jia Y., *Electronic structures and magnetism in Cu-doped ZnO monolayer.* Modern Physics Letters B, 2013. **27**(28): pp. 1-9.
28. Hu K., Wu M., Hinokuma S., Ohto T., Wakisaka M., Fujita J.-i., and Ito Y., *Boosting electrochemical water splitting via ternary NiMoCo hybrid nanowire arrays.* Journal of Materials Chemistry A, 2019. **7**(5): pp. 2156-2164.
29. Pack J.D. and Monkhorst H.J., *" Special points for Brillouin-zone integrations"—a reply.* J Physical Review B, 1977. **16**(4): pp. 1748-1749.
30. Vogel D., Krüger P., and Pollmann J., *Ab initio electronic-structure calculations for II-VI semiconductors using self-interaction-corrected pseudopotentials.* Physical Review B, 1995. **52**(20): pp. 316-319.
31. Razeghi M., *Fundamentals of solid state engineering*. 2006: Springer.
32. Khalil R.A., Hussain M.I., Fatima R., Hussain F., Rana A.M., Hegazy H., and Mera A., *Effect of dopants on the structural, optoelectronic and magnetic properties of pristine AgGaO3 perovskite: A first principles study.* Optik, 2021. **244**: pp. 1-11.
33. Liu Y., Hou Q., Sha S., and Xu Z., *Electronic structure, optical and ferromagnetic properties of ZnO co-doped with Ag and Co according to first-principles calculations.* Vacuum, 2020. **173**: pp. 1-34.
34. Li L., Wang W., Liu H., Liu X., Song Q., and Ren S., *First principles calculations of electronic band structure and optical properties of Cr-doped ZnO.* The Journal of Physical Chemistry C, 2009. **113**(19): pp. 8460-8464.
35. Guo J., Zhou W., Xing P., Yu P., Song Q., and Wu P., *Structural, magnetic and optical properties of vanadium doped zinc oxide: Systematic first-*

principles investigations. Solid state communications, 2012. **152**(11): pp. 924-928.
36. Li Z., Li J., Lei J., Xiong M., Wang N., and Zhang S., *First-principles study of structure, electrical and optical properties of Al and Mo co-doped ZnO.* Vacuum, 2021. **186**: pp. 1-10.
37. Mondal A.K., Mohamed M.A., Ping L.K., Mohamad Taib M.F., Samat M.H., Mohammad Haniff M.A.S., and Bahru R., *First-principles studies for electronic structure and optical properties of p-type calcium doped α-Ga2O3.* Materials, 2021. **14**(3): pp. 1-11.

حسابات نظرية للبنية الإلكترونية والخصائص البصرية لأكسيد الزنك المخدر بالفاناديوم من طريقة الحساب الأساسية الأولى

ريزاو عبدالله قادر[1,2] دلير رفيق صابر[1] شجاع الدين بكرعزيز [1]
[1]قسم الفيزياء، كلية العلوم، جامعة السليمانية، سليمانية، العراق
[2]قسم الفيزياء، كلية التربية، جامعة السليمانية، سليمانية، العراق

الخلاصة

في الدراسة الحالية، تم حساب ثوابت الشبيكة، وتركيب حزمة النطاق، والخصائص البصرية لأوكسيد الزنك (ZnO) النقية والمشوبة بفناديوم (V) من خلال استخدام إمكانات الجهد الكاذب النعومة (USP) وتقريب التدرج المعمم GGA بمساعدة حساب المبادئ الأولية (FPC) المستمدة من نظرية الكثافة الوظيفية (DFT). وقد أجريت القياسات في هندسة الخلايا الفائقة التي تم تحسينها. تم استخدام وتقريب التدرج المعمم -هبرد GGA U +، لجميع النماذج الهندسية، لحساب كمية الطاقة بعد تحسين جميع المعلمات في النماذج. وجدنا ان حجم الأنظمة المطعمة تزداد بزيادة نسبة تطعيم V. تم التحقيق في ZnO النقي والمشوبة بحثا عن فجوات في بنية النطاق ونطاق الطاقة باستخدام تقنيات أخذ العينات K-point الخاصة بمخطط Monkhorst-Pack في اتجاه التماثل العالي لمنطقة بريلوين (G-A-H-K-G-M-L-H). في وجود محتوى V مرتفع، تنخفض طاقة فجوة النطاق الترددي من 3.331eV إلى 2.043 eV كما هو موضح في مخطط النطاق (V.B and C.B). تم دراسة مخططات PDOS و DOS لاكتساب نظرة ثاقبة على البنية الإلكترونية للذرة والكمية التي يساهم فيها كل نطاق طاقة في مدار ذري محدد. مع زيادة نسبة التطعيم V. تم تنفيذ معالجة فجوات النطاق بطريقة تضيق فجوات النطاق، مما أدى إلى حدوث انزياح أحمر في طيف الامتصاص في منطقة الأشعة تحت الحمراء. كما تم توثيق أنه في البداية، أظهرت الدالة الحقيقية والخيالية للوظيفة العازلة زيادة وتلاها انخفاض. تم التحقق من فعالية ذرات V على النفاذية خاصة في المنطقة منخفضة الطاقة من ZnO Perovskite المخدر مقارنة بالنتائج النظرية الأخرى.